Chall. Nano Micro Scale Sci. Tech., 9(1): 1-11, Winter and Spring 2021
DOI: 10.22111/CNMST.2021.38759.1212

ORIGINAL RESEARCH PAPER

Exergy Analysis of a Nanofluid–Based Direct Absorption Solar Collector (DASC) Occupied by Porous Foam

Alireza Hooshmand[1], Iman Zahmatkesh[1], Maryam Karami[2], Shahram Delfani[3]*

[1]*Department of Mechanical Engineering, Mashhad Branch, Islamic Azad University, Mashhad, Iran*
[2]*Department of Mechanical Engineering, Kharazmi University, Tehran, Iran*
[3]*Department of Mechanical Engineering, Road, Housing and Urban Development Research Center, Tehran, Iran*

Received 4 June 2021; revised 18 August 2021; accepted 18 August 2021 available online 2 September 2021

ABSTRACT: In this work, the energy and exergy efficiencies of a nanofluid–based direct absorption solar collector (DASC) are examined experimentally. Attention is focused to analyze the consequences of installation of porous foam in the collector, concentration of the nanoparticles (NPs) in the working fluid, and volumetric flow rate of the nanofluid from the standpoints of the first law and second law of thermodynamics. The porous foam is made up of SiC while the nanofluid contains SiC NPs in water as the base fluid. The results indicate that the foam installation improves both efficiencies. The dominant parameter on the energy efficiency is recorded to be the volumetric flow rate of the nanofluid but the highest contribution on the exergy efficiency belongs to the NPs concentration in the working fluid. More precisely, maximum changes in the exergy efficiency due to the variation in the NPs concentration in the working fluid is recorded to be 63.2%. Meanwhile, it is found that the foam installation and the alternation of the volumetric flow rate of the nanofluid bring 38.2% and 25.3% variations in the exergy efficiency, respectively.

KEYWORDS: *Direct absorption solar collector (DASC); Exergy analysis; Nanofluid; Porous foam*

INTRODUCTION

Owing to the removal of the absorber plate, direct absorption solar collectors (DASCs) have lower thermal resistance in energy absorption than the conventional surface absorption solar collectors. However, conventional fluids employed in DASCs are weak absorbers of solar irradiation. Hence, use of nanofluids in DASCs has been proposed and analyzed in recent years. Otanikar et al. [1] was first who examined the performance of a nanofluid–based DASC. They investigated the effect of graphite, carbon nanotube, and silver water–based nanofluids on the energy efficiency of the collector. The use of the NPs increased the energy efficiency, as compared with the base fluid. Gupta et al. [2] analyzed a DASC operating with the alumina–water nanofluid having the NPs volume fractions of 0.001, 0.005, 0.01, and 0.5%. The addition of the NPs with these concentrations elevated the energy efficiency by 22.1%, 39.6%, 24.6%, and 18.75%, respectively. In another study, Gupta et al. [3] extended this work to investigate the effect of nanofluid flow rate on the energy efficiency. The efficiency was recorded as 8.1% and 4.2% for the nanofluid flow rates of 1.5 and 2 $Lmin^{-1}$, respectively. Karami et al. [4] used copper oxide NPs dispersed in an ethylene glycol–water mixture (30:70) as the working fluid of a DASC and compared the results of the black and reflective interior surfaces. The energy efficiency using the black surface was 4.1% higher than the reflective surface. Also, increasing the volume fraction of the NPs and the nanofluid flow rate improved the energy efficiency. Delfani et al. [5] found that the energy efficiency of a DASC using carbon nanotubes was about 10–29% higher than the base fluid. Vakili et al. [6] discussed the performance of a DASC operating with graphene nanosheets–water nanofluid. At the NPs mass fraction of 0.005% and the nanofluid flow rate of 0.015 kgs^{-1}, the energy efficiency was about 23.3% higher than that of the base fluid. Kilica et al. [7] investigated the use of titanium oxide–water nanofluid on the performance of a DASC. At the NPs volume fraction of 2%, the energy efficiency was reported to be 48.7%. However, it was only 36.2% for pure water. Karami et al. [8] presented a relationship between the optimum energy efficiency and the Nusselt number in a DASC using PVP–coated silver nanofluid as the working fluid. Meanwhile, Karami et al. [9] used Fe_3O_4–SiO_2–water hybrid nanofluid as the working fluid of a DASC. The highest values of the energy efficiency were 73.9%, 79.8%, and 83.7% for the NPs concentrations of 500 ppm, 1000 ppm, and 2000 ppm, respectively. Going into the literature indicates that some authors have performed numerical simulations to analyze the performance of DASCs. Examples are as follows: Iranpour et al. [10]

*Corresponding Author Email: *zahmatkesh5310@mshdiau.ac.ir*
Tel.: +989155109399; Note. This manuscript was submitted on June 4, 2021; approved on August 18; published online September 2, 2021.

Nomenclature

A	surface area of the collector (m^2)	T	temperature (K)
A_i	constant coefficients	T^*	reduced temperature difference (Km^2W^{-1})
A^*	surface area of a section of the DASC perpendicular to the nanofluid flow (m^2)	Tr	transmittance coefficient (m^{-1})
		u	inlet velocity (ms^{-1})
C	specific heat ($Jkg^{-1}K^{-1}$)	U	overall heat transfer coefficient ($Wm^{-2}K^{-1}$)
d_f	fiber diameter of the porous foam (m)		**Greek Letters**
d_p	pore diameter of the porous foam (m)	β	tilt angle of the collector
d_w	window diameter of the porous foam (m)	ε	Porosity
D_h	hydraulic diameter of the collector, $4A^*/P$ (m)	η	energy efficiency
$\dot{E}x$	rate of exergy transfer (W)	η_{ex}	exergy efficiency
f	friction factor	η_{opt}	optical efficiency
g	gravitational acceleration (ms^{-2})	μ	dynamic viscosity ($kgm^{-1}s^{-1}$)
G	solar irradiation on the collector surface (Wm^{-2})	ρ	density ($kg\ m^{-3}$)
		φ	NPs volume fraction (%)
h	enthalpy (Jkg^{-1})		**Subscripts**
h_L	total head loss (m)	amb	Ambient
K_L	local loss coefficient (m)	d	destructed
Ke	extinction coefficient (m^{-1})	f	base fluid
L	length of the collector (m)	i	Inlet
$\dot{m}$	mass flow rate (kgs^{-1})	nf	nanofluid
P	perimeter of a section of the DASC perpendicular to the nanofluid flow (m)	o	Outlet
		p	nanoparticle
PPI	pore per inch	s	Sun
ΔP	pressure drop across the DASC (Pa)		**Abbreviation**
Re	Reynolds number	NPs	nanoparticles
s	entropy ($Jkg^{-1}K^{-1}$)	DASC	direct absorption solar collector

investigated the effect of nanofluid concentration, collector insulation thickness, and the use of absorber plate instead of reflective plate on the performance of a DASC.

With increasing the thickness of the glass, the energy efficiency decreased while raising the thickness of the insulation improved it. Chen et al. [11] carried out a heat transfer analysis and showed that the addition of silver and gold NPs increased the energy efficiency of a DASC more than titanium dioxide ones. This goes back to the fact that the absorption spectra of the silver and gold NPs are more similar to the solar irradiation, than the titanium oxide ones.

Hatami and Jing [12] evaluated the energy efficiency of a nanofluid–based DASC having a wavy absorber plate. In this collector design, the maximum amount of the local Nusselt was higher than the conventional collector. It is noteworthy that the use of nanofluids is not limited to DASCs and they have diverse applications in different types of solar energy systems (e.g., Moravej [13] and Sheikhzadeh et al. [14]). This goes back to their superior optical and thermal properties, compared to pure fluids. An excellent review on the applications of nanofluids in solar energy systems was compiled by Mahian et al. [15] and Wahab et al. [16]. The presence of porous foam inside a thermal system increases the contact surface and improves the heat transfer by disrupting the flow field [17–19]. In spite of that, the foam installation elevates the pressure drop [20]. Meanwhile, the installation of porous foam inside a solar collector increases the heat loss from the collector surface to the ambient substantially, which doubles the necessity of accurate analysis of this issue. It is important to note that the effect of porous foam installation on the performance of DASCs has not been investigated experimentally so far. However, some relating works are as follows:

Valizade et al. [21] measured the transmittance coefficient, the extinction coefficient, and the diffusion distance of CuO and SiC water–based nanofluids as well as porous foams using a spectrophotometer device. In the SiC and CuO nanofluids, increasing the NPs volume fraction from 0.01% to 0.1% elevated the extinction coefficient by 20% and 176%, respectively. In addition, the extinction coefficient in the porous foams increased with decreasing the pore porosity and the pore diameter. In another study, Valizade et al. [22] experimentally evaluated the efficiency of parabolic trough solar collector (PTSC) occupied by a copper porous foam. Experiments

were performed for three collectors with full–porous foam, semi–porous foam, and no porous foam. As a result of the installation of the full–porous foam and the semi–porous foam, the energy efficiency increased by 171.2% and 117.6%, respectively, compared with a conventional PTSC. In another experimental study, Heyhat et al. [23] investigated the increase in thermal efficiency of a DAPTSC using copper oxide–water nanofluid combined with porous foam. At the NPs volume fraction of 0.1%, the collector efficiency increased by about 79.3% when they installed the porous foam. In another attempt, Esmaeili et al. [24] simulated and discussed a DASC occupied by copper oxide foam. Meanwhile, Tonekaboni et al. [25] optimized a solar combined cooling, heating, and power (CCHP) system using porous foam and nanofluid. Additionally, Siavashi et al. [26] numerically studied how the use of nanofluid and porous foam may improve the performance of a PTSC. More recently, Houshmand et al. [27] applied the analysis of variance to the experimental outcomes of a DASC using nanofluid and porous foams. The NPs concentration contributed 31–37% on the energy efficiency while the contribution ratio of the porous foam was 9–12%.

Exergy analysis is a helpful method for design, simulation, and efficiency assessment of energy systems, which complements and improves an energy analysis. This procedure is in widely use for reducing irreversibility and enhancing the efficiency of solar collectors (e.g., Nemati and Javanmardi [28], Golneshan and Nemati [29], Soltani et al. [30], Zamani et al. [31], and Mahian et al. [32]). Hence, it is not surprising to see some previous interests on the exergy analysis of DASCs:

Gorji and Ranjbar [33] performed an exergy analysis to investigate the effect of solar irradiation as well as nanofluid concentration and flow rate on thermal performance of DASCs. The use of graphite and silver NPs improved the energy and exergy efficiencies, as compared with pure water. In another study, Gorji and Ranjbar [34] optimized the energy and exergy efficiencies of DASCs adopting the response surface method. Karami [35] investigated the energy and exergy efficiencies of a DASC operating with hybrid nanofluid. With elevation in the nanofluid concentration, the exergy efficiency increased and after reaching an optimal value, it decreased. Meanwhile, Karami et al. [36] investigated the energy and exergy efficiencies of a new type of DASCs having V–shaped rib roughness elements installed at the bottom of the collector. The maximum value of the energy efficiency for the new collector was up to 16.6% higher than the conventional collector. However, the conventional collector had higher exergy efficiency.

In this study, we perform an exergy analysis for a nanofluid–based residential–type DASC occupied by porous foam and present the corresponding results in conjunction with the outcomes of an energy analysis. The porous foam is made up of SiC while the nanofluid contains SiC NPs in water as the base fluid. To the authors' knowledge, this is the first exergy analysis of a nanofluid–based residential–type DASC occupied by porous foam.

EXPERIMENTAL PROCEDURE

The test system installed in Tehran (35.6961°N, 51.4231°E) is shown in Figure 1. The specifications of the constructed DASC are reported in Table 1. To prevent the possible rise in the heat loss from the glazing due to the installation of the porous foams, a double–walled glass with an air gap of 12 mm was used. Meanwhile, the whole body of the collector was insulated with a 10 mm thick polyurethane insulation.

To receive the maximum amount of solar irradiation, the collector tilt angle was set at 35°. The location of the experimental setup was chosen in a way that free air could easily circulate around the collector. Moreover, there was no shadow or significant reflected irradiation on the collector surface during the tests. Due to the low value of solar irradiation in Tehran, the EN 12975–2 standard [37] was chosen for our solar experiments. The use of this standard also removed the need to perform the tests at different tilt angles. According to this standard, the time required for each test was calculated, which was 14 minutes. The tests were performed under clear sky conditions. For each test, the initial condition was reached by protecting the collector surface against sunlight using a reflective coating. As the solar irradiation reached the minimum value required for the EN 12975–2 standard, the coating was removed quickly. The measurements continued until reaching a steady condition with ±0.1°C variations in the outlet temperature of the collector. It is worth mentioning that errors of the measuring instruments including a pyranometer, the temperature sensors, and a flow meter were ±3.5%, ±0.1°C, and ±1%, respectively.

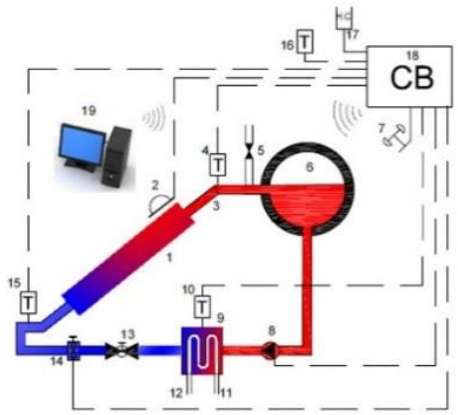

1. Solar collector 2. Pyranometer 3. Insulated pipe
4.Temperature sensor 5. Air vent 6. Collection tank
7. Anemometer 8. Pump 9. Heat exchanger
10.Temperature sensor tank 11. Outgoing water 12. Incoming water
13.Flow control valve 14. Flow meter 15. Temperature sensor
16.Temperature sensor 17.Humidity sensor 18. Control box
19. Computer (PC)

Fig. 1. The experimental setup.

Electrochemical deposition method was used to produce two different porous foams with distinct pore densities (i.e., 10 PPI and 20 PPI). The characteristics of the foams are given in Table 2. Figure 2 shows the samples of the porous foams and their SEM images. Due to the limitations in the production of the porous foams having the height of 2 cm, for both the 10 PPI and 20 PPI foams, six matrices with the dimensions of 10cm×10cm and three matrices with the dimensions of 8cm×10cm were produced. Figure 3 shows the installation of the foams inside the collector.

Table 1
Specifications of the DASC utilized in this study.

Specification	Dimension	Material
Collector length	38 cm	Aluminum
Collector width	38 cm	Aluminum
Aperture length	30 cm	Aluminum
Aperture width	30 cm	Aluminum
Fluid channel depth	2 cm	Aluminum
Glazing (Double wall)	t = 4 mm	Borocilicate glass (Pyrex) (low reflectance) Air gap between two walls: 12 mm
Insulation	t = 1 cm	Polyurethane

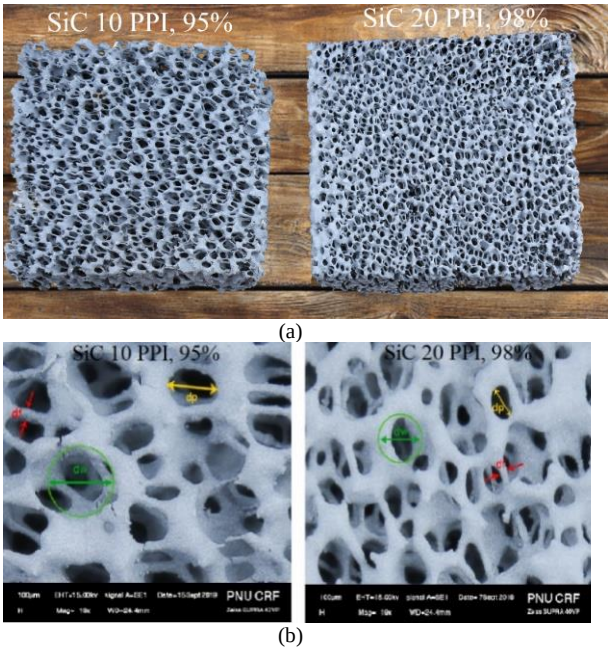

Fig. 2. (a) samples of the SiC porous foams **(b)** SEM images.

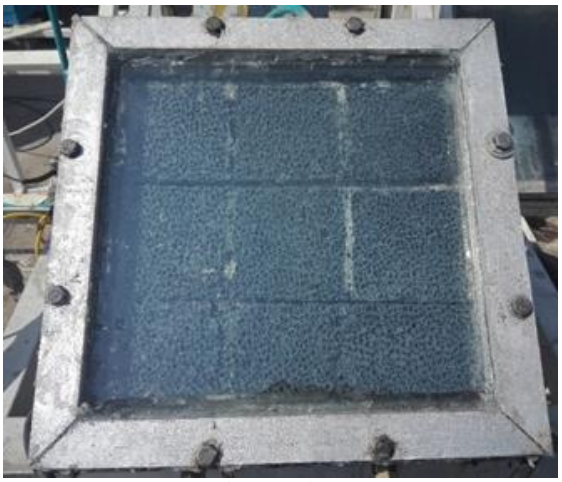

Fig. 3. Installation of the SiC foams inside the DASC.

Table 2
Specifications of the porous foams.

Specifications	Pore density	
	20 PPI	10 PPI
Material	SiC	SiC
Porosity	0.95	0.98
Color	Gray	Gray
Purity	95%	98%
$d_f(mm)$	0.007	0.009
$d_p(mm)$	0.22	0.36
$d_w(mm)$	0.27	0.42

The NPs used in this research were made up of SiC (US Research Nanomaterials, Inc., USA) while the base fluid was the distilled water. The properties of the SiC NPs are

listed in Table 3. Meanwhile, the SEM image of the SiC NPs is depicted in Figure 4(a). To produce the nanofluid, a procedure similar to Sharifi et al. [38] was employed: In the first step, the completely dried NPs were dissolved in distilled water and then, the solution was placed in an ultrasonic device (Elma, Elmasonic, S60H, Germany) for half an hour. In the second step, the Gum Arabic surfactant having the same mass fraction as the NPs was added to the nanofluid and the mixture was placed in the ultrasonic device for another half an hour. In order to increase the ultrasonic efficiency, a hand–made agitator was used to rotate the nanofluid inside the device. Meanwhile, to prevent the possible rise in temperature which may have negative effect on the stability of the nanofluid, for every 15 minutes, the device was turned off for two minutes. This allowed the nanofluid to dissipate the received energy.

Table 3
Specifications of the SiC NPs.

Properties	Value
Shape	Spherical
Relative density	3.22 g/cm^3
Purity	99%
Average diameter of the NPs	65 nm
Color	Gray

Through this two–step procedure, the SiC–water nanofluid was prepared at three different concentrations including 250, 500, and 1000 ppm. The samples were completely stable for at least six months. In Figure 4(b), the photo of the prepared samples in different concentrations is shown. Figure 4(c) presents the particle size distribution performed utilizing a particle size analyzer (Vasco3, Cordouan, France). The value of the zeta potential higher than +30 or lower than –30 is a suitable measure of the nanofluid stability [39]. The zeta potential of the prepared nanofluid lied in this range indicating the appropriate stability of the suspension.

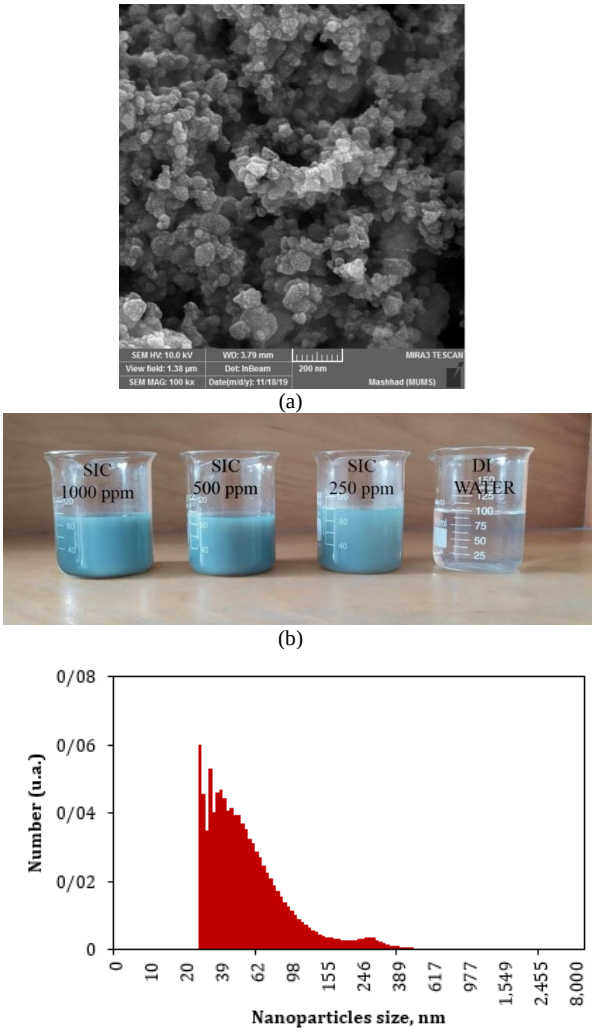

(a)

(b)

(c)

Fig. 4. (a) SEM images of the SiC NPs, **(b)** The SiC nanofluid samples at different concentrations, **(c)** Size distribution of the NPs.

MATHEMATICAL FORMULATION

Energy and exergy efficiencies

The energy efficiency of a DASC is defined as [40]:

$$\eta = \frac{\dot{m} C_{nf} (T_o - T_i)}{A\, G} \tag{1}$$

Here, $\dot{m}$ is the mass flow rate. T_i and T_o are the inlet and outlet temperatures, respectively. A is the collector surface and G is the solar irradiation on the surface of the collector.

Meanwhile, C_{nf} is the specific heat of the nanofluid which is obtained from the following relation:

$$\rho_{nf} C_{nf} = \varphi \rho_p C_p + (1-\varphi)\rho_f C_f \tag{2}$$

with

$$\rho_{nf} = \varphi \rho_p + (1-\varphi)\rho_f \tag{3}$$

Here, φ is the NPs volume fraction. It is noteworthy that in this study, thermophysical properties of the base fluid are calculated at T_m which is the mean temperature of the nanofluid inside the collector (i.e., $T_m = (T_i + T_o)/2$).

Meanwhile, the exergy efficiency of a DASC is defined as [35]:

$$\eta_{ex} = 1 - \frac{\dot{E}x_d}{\dot{E}x_{in}} \quad (4)$$

In the above relation, $\dot{E}x_d$ is the rate of exergy destruction. Meanwhile, $\dot{E}x_{in}$ is the rate of the incoming exergy due to the radiation absorption by the nanofluid which is obtained from the following relation [35]:

$$\dot{E}x_{in} = \eta_{opt} GA\left(1 - \frac{T_{amb}}{T_{sun}}\right) \quad (5)$$

Here, T_{sun} is the apparent sun temperature. Moreover, η_{opt} is the optical efficiency of the DASC which is defined as the percentage of the solar irradiation reaching the glass cover. In this study, similar to Meibodi et al. [41], we take $T_{sun} = 4350$ K and $\eta_{opt} = 0.84$.

For a steady–state system, the exergy balance results in the following equation for the rate of exergy destruction:

$$\dot{E}x_d = \dot{E}x_{heat} - \dot{E}x_{work} + \left(\dot{E}x_{mass,in} - \dot{E}x_{mass,out}\right) \quad (6)$$

The terms in the RHS of the above equation stand for the rates of exergy transfer by the exchanges of heat, work, and mass, respectively.

In a DASC, the exergy transfer rate due to the exchange of heat is obtained from the following equation [41]:

$$\dot{E}x_{heat} = \eta_{opt} GAT_{amb}\left(\frac{1}{T_m} - \frac{1}{T_{sun}}\right) + UA(T_m - T_{amb})\left(1 - \frac{T_{amb}}{T_m}\right) \quad (7)$$

On the other hand, $\dot{E}x_{work}$ in Eq. (6) represents the rate of exergy destruction due to the pressure drop which must be compensated by the pump and is obtained as [41]:

$$\dot{E}x_{work} = -T_{amb}\frac{\dot{m}\Delta P}{\rho_{nf}}\frac{\mathrm{Ln}\left(\frac{T_{out}}{T_{amb}}\right)}{T_{out} - T_{in}} \quad (8)$$

Meanwhile, for the rate of exergy transfer due to the inflow and outflow we have [33]:

$$\dot{E}x_{mass,i} = \dot{m}[(h_{in} - h_{amb}) - T_{amb}(s_{in} - s_{amb})] \quad (9)$$

$$\dot{E}x_{mass,o} = \dot{m}[(h_{out} - h_{amb}) - T_{amb}(s_{out} - s_{amb})] \quad (10)$$

After substitution of Eqs. (7)–(10) into Eq. (6) and some mathematical manipulations, the rate of exergy destruction in a DASC takes the form of:

$$\dot{E}x_d = \eta_{opt} GAT_{amb}\left(\frac{1}{T_m} - \frac{1}{T_{sun}}\right) - \dot{m}C_{nf}(T_{out} - T_{in}) + \dot{m}C_{nf}T_{amb}\,\mathrm{Ln}\left(\frac{T_{out}}{T_{in}}\right) + UA(T_m - T_{amb})\left(1 - \frac{T_{amb}}{T_m}\right) + T_{amb}\frac{\dot{m}\,\Delta P}{\rho_{nf}}\frac{\mathrm{Ln}\left(\frac{T_{out}}{T_{amb}}\right)}{T_{out} - T_{in}} \quad (11)$$

Estimation of pressure drop

Notice in Eq. (11) that for the evaluation of the rate of exergy destruction, pressure drop across the collector must be known. In a conventional DASC, this parameter can be obtained as [41]:

$$\Delta P = \rho_{nf} g(L\,sin\beta + h_L) \quad (12)$$

Here, β is the collector tilt angle and h_L is the total head loss across the collector:

$$h_L = \frac{2\dot{m}}{\rho_{nf} g A^2}\left(f\frac{L}{D_h} + \sum K_L\right) \quad (13)$$

In the above relation, L and D_h are the length and hydraulic diameter of the collector, respectively. f is the friction factor and K_L is the local loss coefficient. For a flat–plate solar collector in the laminar flow regime, the friction factor is: $f = 64/Re$. Meanwhile, the local loss coefficient is equal to 1 at the collector inlet and 1.5 at the collector outlet [35].

For the estimation of pressure drop across the DASC occupied by porous medium, the relation proposed by Kim et al. [42] is adopted as follows:

$$\frac{\Delta P}{L} = \frac{A_1\,\mu_{nf}\,(1-\varepsilon)\,PPI\,u\,d_f}{d_w\,d_p^2} + \frac{A_2\,\rho_{nf}\,(1-\varepsilon)\,u^2}{d_p} \quad (14)$$

Here, ε is the medium porosity. d_f, d_w, and d_p are the fiber diameter, the window diameter, and the pore diameter of the porous foam, respectively. Also, the constant coefficients including A_1 and A_2 are equal to 150 and 2.9, respectively.

Reduced temperature difference

For the evaluation of the performance of the DASC, variations in the energy and exergy efficiencies in terms of the reduced temperature difference, T_m^*, are discussed. This parameter is defined as:

$$T^* = \frac{T_m - T_{amb}}{G} \quad (15)$$

here, T_{amb} is the ambient temperature.

Estimation of the overall heat transfer coefficient

To obtain the overall heat transfer coefficient of the collector, U, according to the EN 12975–2 standard [37], the energy efficiency curve is found through the least squares method as:

$$\eta = \eta_0 - a_1 T^* - a_2 G (T^*)^2 \quad (16)$$

that leads to the coefficient a_1 which is the overall heat transfer coefficient of the collector.

RESULTS AND DISCUSSION

In this section, the outcomes of the energy and exergy analysis for the nanofluid–based direct absorption solar collector occupied by the porous foam are presented and discussed. Attention is focused to explore the effects of the volumetric flow rate of the nanofluid, the concentration of the NPs in the working fluid, and the installation of the porous foam on the energy and exergy efficiencies of the collector.

Firstly, the effect of the volumetric flow rate of the nanofluid on the energy efficiency is examined. To this aim, results belonging to the volumetric flow rates of 15 Lh^{-1}, 30 Lh^{-1}, and 45 Lh^{-1} at three different values of the reduced temperature difference are provided in Figure 6. In a general way notice that rise in the volumetric flow rate improves the energy efficiency. This is attributed to the fact with increase in the flow rate, the fluid temperature decreases within the collector, which attenuates the heat loss from the collector to the ambient elevating the energy efficiency. Closer scrutiny of Figure 6 indicates that the maximum value of efficiency enhancement due to this effect is 43.4%.

To examine the consequence of the NPs concentration in the working fluid on the energy efficiency, Figure 7 is plotted. The figure indicates that addition of the NPs to the working fluid as well as rise in its concentration elevates the energy efficiency. This behavior is not surprising and is accord with previous findings, which is attributed to the improved thermophysical properties of the working fluid. Maximum rise in the energy efficiency due to the addition of the NPs is recorded to be 38.2%.

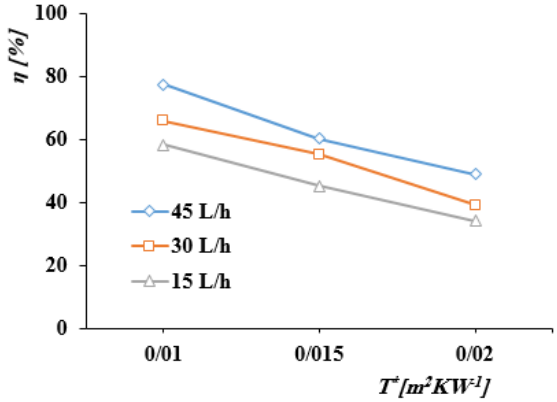

Fig. 6. Effect of the volumetric flow rate of the nanofluid on the energy efficiency.
(10 PPI porous foam, the NPs concentration=500 ppm).

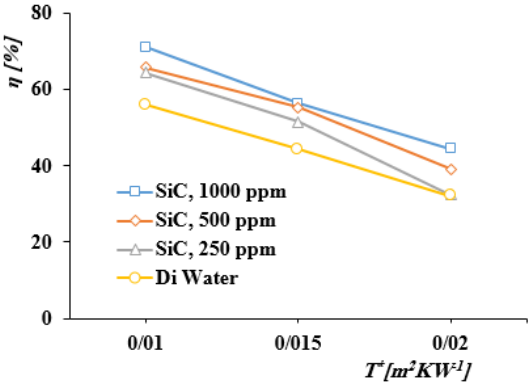

Fig. 7. Effect of the NPs concentration in the working fluid on the energy efficiency .
(10 PPI porous foams, the volumetric flow rate=30 Lh^{-1})

Figure 8 discusses the influence of the installation of the porous foam as well as its pore density on the energy efficiency. It is obvious that the foam installation improves this efficiency. Maximum enhancement in the energy efficiency due to the foam installation is 24.4%. However, notice that no general conclusion can be drawn for the effect of the pore density of the porous foam on the energy efficiency. Although some of the previous works (e.g., Dehghan et al. [43,44]) demonstrate that thermal behavior of porous foam in the case of combined convection–radiation heat transfer follows a predictable procedure, the current observation may not be surprising. Indeed, one expects that any increase in the pore density enhances the heat transfer surface and thereby improves thermal performance. This has also been observed by Hussien and Farhan [45] and Tan et al. [46] in the studies of thermal solar systems. However, numerical simulation of Esmaeili et al. [24] for a DASC shows that rise in the pore density may establish a high temperature zone near

the upper wall of the collector which intensifies thermal loss and decreases the energy efficiency. Hence, the observed unpredictable procedure for the effect of the pore density of the porous foam on the energy efficiency is expected.

Now, the outcomes of the exergy analysis are outlined. To this aim, Figures 9 and 10 are plotted showing the effect of the volumetric flow rate of the nanofluid and the NPs concentration in the working fluid on the exergy efficiency, respectively. It is obvious that no general trend can be reached for the both effects. However, inspection of Figure 9 demonstrates that the volumetric flow rates of 30 Lh^{-1} and 45 Lh^{-1} lead to higher exergy efficiencies, as compared to that of 15Lh^{-1}. Notice in Figure 10 that in some cases, the exergy efficiency of the SiC nanofluid is even lower than the DI water. This goes back to the increased fluid viscosity which elevates pressure drop across the DASC and indicates that in some cases, the NPs addition may not be a good strategy for the performance improvement of the current DASC from the standpoint of the second law of thermodynamics. Maximum variations in the exergy efficiency due to the change in the volumetric flow rate of the nanofluid and the NPs concentration in the working fluid are found to be 25.3% and 63.2%, respectively.

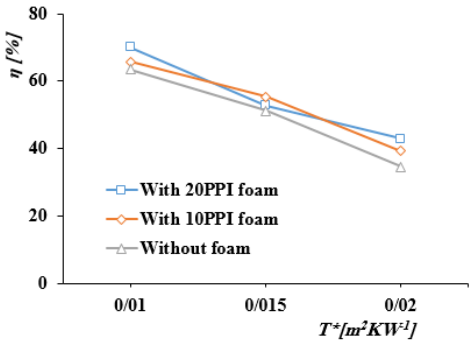

Fig. 8. Effect of installation of the porous foam and its pore density on the energy efficiency (the NPs concentration=500 ppm, the volumetric flow rate=30 Lh^{-1}).

Finally, Figure 11 is plotted to portray how the installation of the porous foam as well as its pore density may affect the exergy efficiency. It is obvious that the foam installation has positive effect on the exergy efficiency. However, similar to the energy efficiency, no general conclusion can be drawn for the effect of the pore density of the foam on the exergy efficiency. It is noticed that maximum rise in the exergy efficiency due to the foam installation is 38.2%.

Scrutiny of Figures 9–11 shows that no general trend can be reached for the effects of the volumetric flow rate of the nanofluid, the concentration of the NPs in the working fluid, and the installation of the porous foam on the exergy efficiency of the collector. Owing to the complex relation between each of these parameters and the exergy destruction (i.e., Equation (11)), this is expected. For instance, notice that any rise in the volumetric flow rate of the nanofluid (a) increases the rate of exergy transfer due to the inflow and outflow, (b) attenuates the exergy transfer rate due to the exchange of heat as a result of decrease in the fluid temperature within the collector, and (c) elevates exergy destruction due to the pressure drop. Since the relative importance of these competing effects are not similar under different conditions, a predictable procedure for the effect of the volumetric flow rate of the nanofluid on the exergy efficiency cannot be reached.

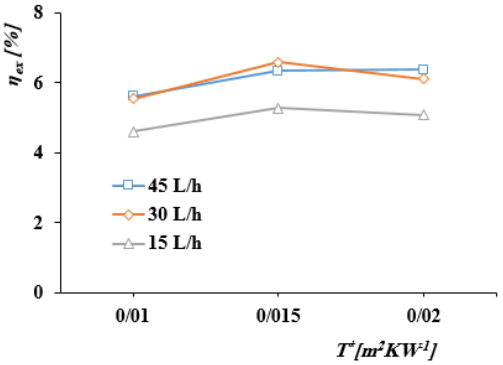

Fig. 9. Effect of the volumetric flow rate of of the nanofluid on the exergy efficiency
(10 PPI porous foam, the NPs concentration=500 ppm).

CONCLUSION

Results of an exergy analysis for a nanofluid–based direct absorption solar collector occupied by porous foam in conjunction with the outcomes of an energy analysis were presented and discussed in this study. Based on the presented results, the following conclusions may be drawn:

1) Rise in the volumetric flow rate of the nanofluid or the NPs concentration in the working fluid elevates the energy efficiency. Maximum value of the energy efficiency enhancement due to these two effects are 43.4% and 38.2%, respectively. Hence, the dominant parameter on the energy efficiency is the volumetric flow rate of the nanofluid.
2) No predictable procedure for the effect of the volumetric flow rate of the nanofluid or the NPs concentration in the working fluid on the exergy efficiency is achievable in a way that in some cases, the exergy efficiency of the SiC nanofluid is even lower than the DI water. However, maximum variations in the exergy efficiency due to the change in the volumetric flow rate of the nanofluid and the NPs concentration in the working fluid are 25.3% and 63.2%, respectively. Thereby, the highest contribution on the exergy

efficiency belongs to the NPs concentration in the working fluid.

3) The installation of the porous foam improves the energy and exergy efficiencies. However, no general conclusion can be found for the effect of the pore density of the foam on these efficiencies.

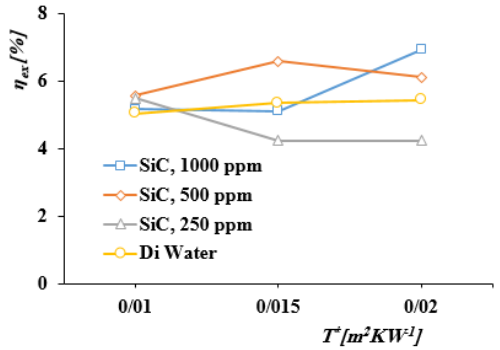

Fig. 10. Effect of the NPs concentration in the working fluid on the exergy efficiency
(10 PPI porous foam, the volumetric flow rate=30 Lh^{-1})

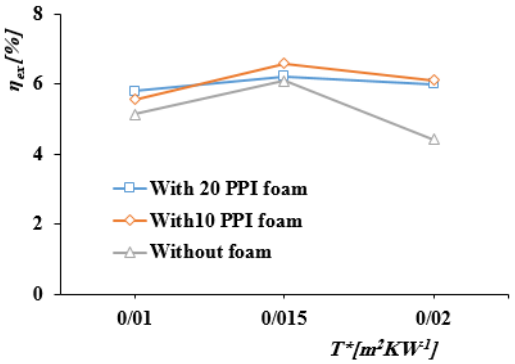

Fig. 11. Effect of installation of the porous foam and its pore density on the exergy efficiency. (The NPs concentration=500 ppm, the volumetric flow rate=30 Lh^{-1})

CONFLICTS OF INTERESTS

The authors declared no potential conflicts of interest with respect to the research, authorship, and/or publication of this article.

REFERENCES

[1] Otanicar TPP, Phelan E, Prasher RS, Rosengarten G, Taylor RA. Nanofluid–based direct absorption solar collector, J. Renew. Sustain. Energy, 2010, 2, 33102–33120

[2] Gupta HK, Agrawal GD, Mathur J. An experimental investigation of a low temperature Al_2O_3–H_2O nanofluid based direct absorption solar collector, Sol. Energy, 2015, 118, 390–396.

[3] Gupta HK, Agrawal GD, Mathur J. Investigations for effect of Al_2O_3–H_2O nanofluid flow rate on the efficiency of direct absorption solar collector, Case Stud. Therm. Eng., 2015, 5, 70–78.

[4] Karami M, Akhavan–Bahabadi MA, Delfani S, Raisee S. Experimental investigation of CuO nanofluid–based direct absorption solar collector for residential applications, Renew. Sustain. Energy Rev., 2015, 52, 793–801.

[5] Delfani S, Karami S, Akhavan–Behabadi MA. Performance characteristics of a residential–type direct absorption solar collector using MWCNT nanofluid, Renew. Energy, 2016, 87, 754–764.

[6] Vakili M, Hosseinalipour SM, Delfani S, Khosrojerdi S. Karami M, Experimental investigation of graphene nanoplatelets nano fluid–based volumetric solar collector for domestic hot water systems, Sol. Energy, 2016, 131, 119–130.

[7] Kiliça F, Menlik T, Sözen A. Effect of titanium dioxide–water nanofluid use on thermal performance of the flat plate solar collector, Sol. Energy, 2018, 164, 101–108.

[8] Karami M, Bozorgi M, Delfani S, Akhavan–Behabadi MA. Empirical correlations for heat transfer in a silver nanofluid–based direct absorption solar collector, Sustain. Energy Technol. Assess., 2018, 12, 14–21.

[9] Karami M, HosseiniPakdel SM, Delfani S, Akhavan–Behabadi MA. Application of Fe_3O_4–silica hybrid nanofluid as working fluid of direct absorption solar collector, Modares Mech. Eng., 2018, 18, 37–44.

[10] Iranpour AK, Karami M, Delfani S. Numerical investigations of the influence of effective parameters on efficiency of DASC with CuO–H_2O nanofluid, J. Solid Fluid. Mech., 2017, 7, 91–100.

[11] Chen M, He Y, Zhu J, Wen D. Investigating the collector efficiency of silver nanofluids based direct absorption solar collectors, Appl. Energy, 2016, 181, 65–74.

[12] Hatami M, Jing D. Evaluation of wavy direct absorption solar collector (DASC) performance using different nanofluids, J. Mol. Liq., 2017, 229, 203–211.

[13] Moravej M. Efficiency enhancement in a triangular solar flat plate collector by using Al_2O_3–water nanofluids: An experimental study, Chall. Nano Micro Scales Sci. Tech., 2020, 8, 99–108.

[14] Sheikhzadeh GA, Monfaredi F, Aghaei A, Sadripour S, Doakhan E, Adibi M. Numerical analysis of thermal–hydraulic properties of turbulent aerosol–carbon black nanofluid flow in

corrugated solar collectors with double application, Chall. Nano Micro Scales Sci. Tech., 2019, 7, 37–52.

[15] Mahian O, Kianifar A, Kalogirou SA, Pop I, Wongwises S. A review of the applications of nanofluids in solar energy, Int. J. Heat Mass Transf., 2013, 57, 582–594.

[16] Wahab A, Hassan A, Qasim MA, Ali HM, Babar H, Sajid MU. Solar energy systems – Potential of nanofluids, J. Mol. Liq., 2019, 289, 111049.

[17] R. A Mohamed., A. M. Aly., S. E. Ahmed. and M. S. Soliman., MHD Jeffrey nanofluids flow over a stretching sheet through a porous medium in presence of nonlinear thermal radiation and heat heneration/absorption, Chall. Nano Micro Scales Sci. Tech., 2020, 8, 9–22.

[18] Sobamowo GM, Akinshilo A, Yinusa AA. Two–dimensional flow analysis of nanofluid through a porous channel with suction/injection at slowly expanding/contracting walls using variation of parameter method, Chall. Nano Micro Scales Sci. Tech., 2019, 7, 120–129.

[19] Goli A, Zahmatkesh I. Slip flow in porous micro–tubes under local thermal non–equilibrium conditions, Chall. Nano Micro Scales Sci. Tech., 2018, 6, 79–87.

[20] Bazkhane S, Zahmatkesh I. Taguchi–based sensitivity analysis of hydrodynamics and heat transfer of nanofluids in a microchannel heat sink (MCHS) having porous substrates, Int. Commun. Heat Mass Transf. 2020, 118, 104885.

[21] Valizade M, Heyhat MM Maerefat M. Experimental comparison of optical properties of nanofluid and metal foam for using in direct absorption solar collectors, Sol. Energy Mater. Sol. Cells, 2019, 195, 71–80.

[22] Valizade M, Heyhat MM, Maerefat M. Experimental study of the thermal behavior of direct absorption parabolic trough collector by applying copper metal foam as volumetric solar absorption, Renew. Energy, 2020, 145, 261–269.

[23] Heyhat MM, Valizade M, Abdolahzade Sh. Maerefat M. Thermal efficiency enhancement of direct absorption parabolic trough solar collector (DAPTSC) by using nanofluid and metal foam, Energy 2020, 192, 116662.

[24] Esmaeili M, Karami M, Delfani S. Performance enhancement of a direct absorption solar collector using copper oxide porous foam and nanofluid, Int. J. Energy Res. 2020, 44, 5527–5544.

[25] Tonekaboni N, Feizbahar M, Tonekaboni N, Jiang GJ, Chen HX, Optimization of solar CCHP systems with collector enhanced by porous media and nanofluid, Math. Probl. Eng., 2021, 9984840.

[26] Siavashi M, Bozorg MV, Toosi MH. A numerical analysis of the effects of nanofluid and porous media utilization on the performance of parabolic trough solar collectors, Sustain. Energy Technol. Assess., 2021, 45, 101179.

[27] Hooshmand A, Zahmatkesh I, Karami M, Delfani S. Porous foams and nanofluids for thermal performance improvement of a direct absorption solar collector: An experimental study, Environ. Prog. Sustain. Energy (In Press). DOI: 10.1002/ep.13684.

[28] Nemati H, Javanmardi MJ. Exergy optimization of domestic solar cylindrical–parabolic cooker, J. Renew. Sustain. Energy, 2012, 4, 063134.

[29] Golneshan AA, Nemati H. Exergy analysis of unglazed transpired solar collectors (UTCs), Sol. Energy, 2014, 107, 272–277.

[30] Soltani S, Kasaeian A, Lavajoo A, Loni R, Najafi G, Mahian O. Exergetic and enviromental assessment of a photovoltaic thermal–thermoelectric system using nanofluids: Indoor experimental tests, Energy Convers. Manag., 2020, 218, 112907.

[31] Zamani H, Mahian O, Rashidi I, Lorenzini G, Wongwises S. Exergy optimization of a double–exposure solar cooker by response surface method, J. Therm. Sci, Eng. Appl., 2017, 9, 011003.

[32] Mahian O, Kianifar A, Heris SZ, Wongwises S. First and second law analysis of a mini–channel based solar collector using boehmite alumina nanofluids: Effects of nanoparticle shape and tube materials, Int. J. Heat Mass Transf., 2014, 78, 1166–1176.

[33] Gorji TB, Ranjbar AA. A numerical and experimental investigation on the performance of a low–flux direct absorption solar collector (DASC) using graphite, magnetite and silver nanofluids, Sol. Energy, 2016, 135, 493–505.

[34] Gorji TB, Ranjbar AA. Thermal and exergy optimization of a nanofluid–based direct absorption solar collector, Renew. Energy, 2017, 106, 274–287.

[35] Karami M. Experimental investigation of first and second laws in a direct absorption solar collector using hybrid Fe_3O_4–SiO_2 nanofluid, J. Therm. Anal. Calorim., 2018, 136, 1–11.

[36] Karami M, Delfani S, Esmaeili M. Effect of V–shaped rib roughness on the performance of nanofluid based direct absorption solar collectors, J. Therm. Anal. Calorim., 2019, 138, 559–572.

[37] EN 12975–2, Thermal Solar Systems and Components – Solar Collectors – Part 2: Test Methods, 2001.

[38] Sharifi AH, Zahmatkesh I, Mozhdehi AM, Morsali A, Bamoharram FF. Stability appraisement of the alumina–brine nanofluid in the presence of ionic and non–ionic disparents on the alumina nanoparticles surface as heat transfer fluids: Quantum mechanical study and Taguchi–optimized experimental analysis, J. Mol. Liq., 2020, 319, 113898.

[39] Choudhary R, Khurana D, Kumar A, Subudhi S. Stability analysis of Al_2O_3/water nanofluids, J. Exp. Nanosci., 2017, 12, 140–151.

[40] Fischer S, Heidemann W, Müller–Steinhagen H, Perers B, Bergquist P, Hellström B. Collector test method under quasi–dynamic conditions according to the European Standard EN 12975–2, Sol. Energy, 2004, 76, 117–123.

[41] Meibodi SS, Kianifar A, Mahian O, Wongwises S. Second law analysis of a nanofluid–based solar collector using experimental data, J. Therm. Anal. Calorim., 2016, 126, 617–625.

[42] Kim D, Kim KC. An experimental study on the thermal and hydraulic characteristics of open–cell nickel and copper foams for compact heat exchangers, Int. J. Heat Mass Transf., 2019, 130, 162–174.

[43] Dehghan M, Mahmoudi Y, Valipour MS, Saedodin S. Combined conduction–convection–radiation heat transfer of slip flow inside a micro–channel filled with a porous material, Transp. Porous Med., 2015, 108, 413–436.

[44] Dehghan M, Rahmani Y, Ganji DD, Saedodin S, Valipour MS, Rashidi S. Convection–radiation heat transfer in solar heat exchangers filled with a porous medium: Homotopy perturbation method versus numerical analysis, Renew. Energy, 2015, 74, 448–455.

[45] Hussien SQ, Farhan AA. The effect of metal foam fins on the thermo–hyraulic performance of a solar air heater, Int. J. Renew. Energy Res., 2019, 9, 840–847.

[46] Tan WC, Saw LH, Yusof F, Thiam HS, Xuan J. Investigation of functionally graded metal foam thermal management system for solar cell, Int. J. Energy Res., 2020, 44, 9333–9349.